Inorganic Chemistry

Article

pubs.acs.org/IC

Biotinylated Platinum(II) Ferrocenylterpyridine Complexes for Targeted Photoinduced Cytotoxicity

Koushambi Mitra,[†] Abhijith Shettar,[‡] Paturu Kondaiah,*[,‡] and Akhil R. Chakravarty*[,†]

[†]Department of Inorganic and Physical Chemistry and [‡]Department of Molecular Reproduction, Development and Genetics, Indian Institute of Science, Bangalore 560012, India

Supporting Information

ABSTRACT: Biotinylated platinum(II) ferrocenylterpyridine (Fc-tpy) complexes [Pt(Fc-tpy)(L^1)]Cl (**1**) and [Pt(Fc-tpy)(L^2)]Cl (**2**), where HL^1 and HL^2 are biotin-containing ligands, were prepared, and their targeted photoinduced cytotoxic effect in cancer cells over normal cells was studied. A nonbiotinylated complex, [Pt(Fc-tpy)(L^3)]Cl (**3**), was prepared as a control to study the role of the biotin moiety in cellular uptake properties of the complexes. Three platinum(II) phenylterpyridine (Ph-tpy) complexes, viz., [Pt(Ph-tpy)(L^1)]Cl (**4**), [Pt(Ph-tpy)(L^2)]Cl (**5**), and [Pt-(Ph-tpy)(L^3)]Cl (**6**), were synthesized and explored to understand the role of a metal-bound Fc-tpy ligand over Ph-tpy as a photoinitiator. The Fc-tpy complexes displayed an intense absorption band near 640 nm, which was absent in their Ph-tpy analogues. The Fc-tpy complexes (1 mM in 0.1 M TBAP) showed an irreversible cyclic voltammetric anodic response of the Fc/Fc^+ couple near 0.25 V. The Fc-tpy complexes displayed photodegradation in red light of 647 nm involving the formation of a ferrocenium ion (Fc^+) and reactive oxygen species (ROS). Photoinduced release of the biotinylated ligands was observed from spectral measurements, and this possibly led to the controlled generation of an active platinum(II) species, which binds to the calf-thymus DNA used for this study. The biotinylated photoactive Fc-tpy complexes showed significant photoinduced cytotoxicity, giving a IC_{50} value of ~7 μM in visible light of 400−700 nm with selective uptake in BT474 cancer cells over HBL-100 normal cells. Furthermore, ferrocenyl complexes resulted in light-induced ROS-mediated apoptosis, as indicated by DCFDA, annexin V/FITC staining, and sub-G1 DNA content determined by fluorescent activated cell sorting analysis. The phenyl analogues **4** and **5** were photostable, served as DNA intercalators, and demonstrated selective cytotoxicity in the cancer cells, giving IC_{50} values of ~4 μM.

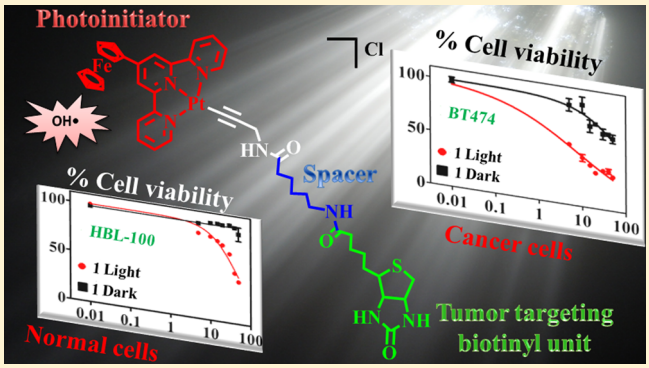

1. INTRODUCTION

Site-directed delivery and controlled activation of an anticancer agent are the major challenges to potentiate its clinical applications. The conventional treatment modalities such as chemotherapy or radiotherapy suffer from high systemic toxicity along with the associated risks of metastatic cancer growth. Photodynamic therapy (PDT) has emerged as an alternate methodology in which a photosensitizer that is inactive and nontoxic in the dark selectively damages the photoexposed cancer cells, leaving the unexposed healthy cells unaffected.[1−5] In addition to selectivity, the efficacy of a PDT agent can be increased by targeting cancer cells over normal cells. Tumor cells with enhanced metabolic rates and leaky vasculature have preferential accumulation of the photosensitizers over normal cells. However, the presence of some highly proliferating normal cells like red blood cells, gut epithelia, bone marrow, and hair follicles enhances the nonspecific uptake of the drug, thus requiring high drug doses that lead to unwanted adverse effects. Thus, a targeted drug-delivery system (DDS) assumes great importance for augmented cellular uptake of the drug in cancer cells over healthy cells.[6−8] DDS reduces both the drug dosage and the amount of drug circulating in body fluids. DDS can be suitably designed with the knowledge that cancer cells overexpress receptors to aid internalization of growth-promoting factors like vitamins, glucose, peptides, antibodies, and hormones.[9−12] For example, drug conjugates with biotin, riboflavin, vitamin B12, and folic acid are known to show cancer-cell-specific uptake.[13−15] We have chosen biotin, which is known as vitamin H or vitamin B7 and is extensively used for tumor targeting, for our study. In vitro and in vivo literature reports indicate that uptake of biotin is facilitated by sodium-dependent multivitamin transporters (SMVTs), which are overexpressed in certain cancer cell lines.[16−19] The strong affinity of biotin for protein receptors like avidin and streptavidin (~10^{14} M) is well explored.[20] Taxoids, gemcitabine, doxorubicin, annonaceous acetogenins, and p53 proteins, when conjugated to biotin, have shown selective delivery to cancer cells without affecting their cytotoxic effects.[16,21,22] Kim and co-workers have reported

Received: March 18, 2016

DOI: 10.1021/acs.inorgchem.6b00680
Inorg. Chem. XXXX, XXX, XXX−XXX

several biotin−drug conjugates as tumor-targeted theranostic and bioimaging probes.[23−25]

The present work stems from our interest to develop platinum(II)-based PDT agents using a biotinylated acetylide ligand for their targeted delivery to tumor cells rather than to normal ones (Figure 1). We have chosen platinum as the metal

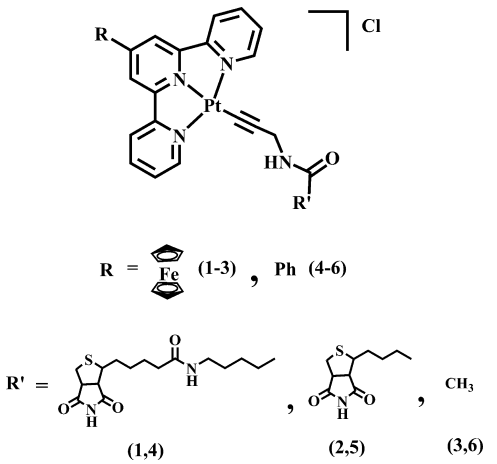

Figure 1. Molecular structures of complexes **1**−**6**.

considering the successful use of this metal-based drug, viz., cisplatin, carboplatin, and oxaliplatin, as a novel chemotherapeutic agent.[26−28] Although few platinum(IV) complexes are used in photoactivated chemotherapy, the potential of platinum(II) complexes in PDT is yet to be realized.[29−35] Platinum complexes show excellent photophysical properties with enhanced triplet-state population upon excitation due to spin−orbit coupling, and photoactive platinum complexes could serve as attractive candidates for PDT. In addition, ligand dissociation from ruthenium and platinum complexes in their excited states often results in dual photochemotherapeutic effects, which offer an oxygen-independent mechanistic action suitable for the treatment of hypoxic solid tumors.[36,37] We have earlier shown that platinum(II) ferrocenylterpyridine (Fc-tpy) complexes are significantly photocytotoxic in cancer cells with low dark toxicity.[33] The Fc-tpy moiety upon binding to platinum(II) behaves as an excellent photoinitiator within the PDT spectral window (600−800 nm) and generates reactive oxygen species (ROS), which causes cellular damage. With an objective to develop the virtually unexplored PDT chemistry of platinum(II) complexes, we have designed and synthesized new ternary Pt^{II}(Fc-tpy) complexes of biotin-conjugated acetylide ligands HL^1 and HL^2, viz., [Pt(Fc-tpy)(L^1)]Cl (**1**) and [Pt(Fc-tpy)(L^2)]Cl (**2**), where HL^1 is 6-[5-(2-oxohexahydro-1*H*-thieno[3,4-*d*]imidazol-4-yl)pentanamido]-*N*-(prop-2-yn-1-yl)-hexanamide and HL^2 is 5-(2-oxohexahydro-1*H*-thieno[3,4-*d*]imidazol-4-yl)-*N*-(prop-2-yn-1-yl)pentanamide (Figure 1). Complex **1** has an acetylide biotin unit bound to the Pt^{II}(Fc-tpy) moiety, while it is separated with a 6-aminocaproic acid linker in complex **2**. A nonbiotinylated complex, [Pt(Fc-tpy)(L^3)]Cl (**3**), where HL^3 is *N*-(prop-2-yn-1-yl)acetamide, was prepared to investigate the role of the biotin unit in **1** and **2**. Three other complexes, viz., [Pt(Ph-tpy)(L^1)]Cl (**4**), [Pt(Ph-tpy)(L^2)]Cl (**5**), and [Pt(Ph-tpy)(L^3)]Cl (**6**), were prepared and studied to understand the role of the Fc-tpy and Ph-tpy ligands as photosensitizers in **1**−**6**. The significant results from this study include (i) impressive photoinduced cytotoxicity of complex **1** in visible light (400−700 nm) in human breast cancer cells (BT474) while remaining nontoxic in the dark (IC_{50} value: 7 μM in light and >50 μM in the dark), (ii) nominal toxicity in human normal breast cell lines HBL-100 (IC_{50} in light: ∼45 μM), (iii) the Ph-tpy complexes showing undesirable dark toxicity and no apparent PDT effect, highlighting the importance of the Fc-tpy moiety in the photoactivation process, (iv) the biotinylated Ph-tpy complex showing significant cytotoxicity in the dark (IC_{50} value: ∼4 μM), indicating the importance of SMVT in enhancing the cellular uptake, and (v) increased uptake of biotin-conjugated complexes in cancer cells than in normal cells.

2. EXPERIMENTAL SECTION

Materials and Measurements. The chemicals and reagents were procured from commercial sources. Dulbecco's phosphate-buffered saline (DPBS), calf-thymus (ct)-DNA, agarose (molecular biology grade), catalase, superoxide dismutase (SOD), ethidium bromide (EB), 3-(4,5-dimethylthiazol-2-yl)-2,5-diphenyltetrazolium bromide (MTT), and 2′,7′-dichlorofluorescein diacetate (H_2DCFH-DA) were purchased from Sigma-Aldrich, USA. Potassium tetrachloroplatinate and supercoiled (SC) pUC19 DNA (cesium chloride purified) were obtained from Arora Matthey (India) and Bangalore Genie (India), respectively. Tetrabutylammonium perchlorate (TBAP) was synthesized using tetrabutylammonium bromide and perchloric acid. Ligands HL^1, 6-biotinylaminocaproic acid, and HL^2 and the precursor complexes [Pt(Fc-tpy)Cl]Cl and [Pt(Ph-tpy)Cl]Cl were synthesized following reported methods.[33,38,39] The ligands were synthesized using amide-coupling reactions with anhydrous hydroxybenzotriazole (HOBt) and 1-ethyl-3-(3-(dimethylamino)propyl)carbodiimide (EDCI) as the coupling reagents. The crude product was column-chromatographed to obtain pure ligands in moderate yields (∼40%). Synthetic details and characterization data are given as Supporting Information (Scheme S1 and Figures S1−S3).

Elemental analysis, high-performance liquid chromatography (HPLC), UV−visible, emission, IR, molar conductivity, and mass (MS) and NMR spectral measurements were done using equipment that was reported earlier.[34] Cyclic voltammograms were recorded using an EG&G PAR model 253 VersaStat potentiostat/galvanostat equipped with electrochemical analysis software 270. A three-electrode setup, consisting of a glassy carbon working electrode, a platinum wire counter electrode, and a saturated calomel (SCE) pseudoreference electrode, was used [***Caution!*** *mercury and its salts, being highly toxic, were handled with proper safety precautions*]. Potentials were finally corrected versus Fc/Fc^+ by keeping ferrocene as an internal standard. Solid-state emission spectra were recorded using an Edinburgh FLS920 spectrometer. A Becton Dickinson fluorescent activated cell sorting (BD-FACS) Verse configured with three lasers (405 nm, 40 mW; 488 nm, 20 mW; and 640 nm, 40 mW) and an eight-parameter Windows 7 operating system with BD-FACS suite software for acquisition and analysis was used for FACS analysis. An inductively coupled plasma mass spectroscopy (ICP-MS) method was used to evaluate the platinum content by ICP-MS, Thermo X series II. A Waters Alliance System equipped with *EMPOWER 3* software (Waters Corp., Milford, MA; 2695 separation module, 2996 photodiode-array detector) was employed to perform HPLC. The 30 μL solutions (5 mM) were run in aqueous methanol (MeOH) while the MeOH percentage was maintained as 95% for 17 min and 5% for 8 min. A reversed-phase column (Lichrosphere 60, RP-select B, 5 mm, flow rate of 1 mL min^{-1}) was used, and all of the samples were detected at 275 nm.

Synthesis of Complexes 1−6. The complexes were prepared by following a general synthetic procedure. To a *N*,*N*-dimethylformamide (DMF) solution (2 mL) of the ligand (HL^1, 94 mg, 0.24 mmol for **1** and 118 mg, 0.3 mmol for **4**; HL^2, 67 mg, 0.24 mmol for **2** and 83 mg, 0.3 mmol for **5**; HL^3, 30 mg, 0.3 mmol for **3** and 40 mg, 0.41 mmol for **6**) was added freshly distilled triethylamine (5 mL), and the solution was stirred for 1 h under a nitrogen atmosphere. To this solution was

DOI: 10.1021/acs.inorgchem.6b00680
Inorg. Chem. XXXX, XXX, XXX−XXX

added the precursor complex [Pt(Fc-tpy)Cl]Cl (0.08 g, 0.12 mmol) for **1**−**3** and [Pt(Ph-tpy)Cl]Cl (0.08 g, 0.14 mmol) for **4**−**6**, taken in dry DMF (8 mL) along with a catalytic amount of CuI (5 mg). The resulting mixture was stirred for 48 h in the dark and then filtered. The desired complex was precipitated by adding diethyl ether, dried, and reprecipitated from an acetonitrile (MeCN) solution by adding diethyl ether to obtain the product in an analytically pure form. The characterization data are given below.

[Pt(Fc-tpy)(L^1)]Cl (**1**). Yield: 110 mg, ∼88%. Anal. Calcd for $C_{44}H_{48}ClFeN_7O_3PtS$: C, 50.75; H, 4.65; N, 9.42. Found: C, 50.55; H, 4.89; N, 9.40. ESI-MS in MeOH: *m*/*z* 1005.2538 ([M − Cl]$^+$; 100%). ^{1}H NMR (400 MHz, DMSO-d_6): δ 9.14 (d, 2H), 8.82 (d, 2H), 8.68 (s, 2H), 8.55 (m, 2H), 8.19 (b, 1H), 7.89 (m, 2H), 7.72 (b, 1H), 6.45 (s, 1H), 6.30 (s, 1H), 5.43 (d, 2H), 4.80 (s, 2H), 4.22 (s, 1H), 4.18 (s, 5H), 4.17 (b, 3H), 3.07 (m, 1H), 2.99 (m, 2H), 2.80 (s, 1H), 2.5 (s, 1H), 2.15 (m, 2H), 2.13 (m, 2H), 1.49−1.25 (b, 12H) [b, broad; s, singlet; d, doublet; m, multiplet]. UV−visible in 10% DMSO−DPBS (pH = 7.2) [λ_{max}, nm (ε, M^{-1} cm^{-1})]: 640 (2700), 455 (3400), 345 (10000), 282 (17000). IR data in the solid phase (cm^{-1}): 3240 m, 3064 m, 2915 m, 2859 m, 2181 w, 2068 w, 1983 w, 1688 s, 1639 s, 1602 s, 1539 s, 1431 m, 1241 m, 780 w, 725 w, 669 w, 498 m, 470 m [s, strong; m, medium; w, weak]. Λ_M, S m^2 M^{-1} in DMF at 25 °C: 65.

[Pt(Fc-tpy)(L^2)]Cl (**2**). Yield: 95 mg, ∼85%. Anal. Calcd for $C_{38}H_{37}ClFeN_6O_2PtS$: C, 49.17; H, 4.02; N, 9.05. Found: C, 48.88; H, 4.22; N, 9.11. ESI-MS in MeOH: *m*/*z* 892.1653 ([M − Cl]$^+$, 100%). ^{1}H NMR (400 MHz, DMSO-d_6): δ 8.90 (m, 2H), 8.77 (m, 2H), 8.59 (m, 2H), 8.47 (m, 2H), 8.22 (b, 1H), 7.95−7.88 (b, 2H), 6.45 (s, 1H), 6.38 (s, 1H), 5.44 (d, 2H, *J* = 12 Hz), 4.81 (d, 2H, *J* = 8 Hz), 4.29 (m, 1H), 4.23 (s, 5H), 4.20 (b, 3H), 3.09 (m, 1H), 2.81 (m, 1H), 2.58 (m, 1H), 2.18 (b, 2H), 1.60−1.11 (b, 6H). UV−visible in 10% DMSO−DPBS (pH = 7.2) [λ_{max}, nm (ε, M^{-1} cm^{-1})]: 642 (2900), 462 (3400), 350 (9000), 265 (25000). IR data in solid phase (cm^{-1}): 3261 s, 3229 s, 3063 s, 2920 s, 1687 s, 1643 s, 1604 s, 1543 s, 1432 m, 1246 m, 1163 w, 783 w, 576 w, 501 m, 478 m. Λ_M, S m^2 M^{-1} in DMF at 25 °C: 70.

[Pt(Fc-tpy)(L^3)]Cl (**3**). Yield: 80 mg, ∼89%. Anal. Calcd for $C_{30}H_{25}ClFeN_4OPt$: C, 48.44; H, 3.39; N, 7.53. Found: C, 48.58; H, 3.45; N, 7.41. ESI-MS in MeOH: *m*/*z* 708.1064 ([M − Cl]$^+$, 100%). ^{1}H NMR (400 MHz, DMSO-d_6): δ 9.13 (m, 2H), 8.98 (m, 2H), 8.82 (b, 2H), 8.67 (b, 2H), 8.57 (b, 1H), 7.90 (b, 2H), 5.45 (d, 2H, *J* = 8 Hz), 4.83 (d, 2H, *J* = 12 Hz), 4.22 (s, 5H), 4.21 (s, 2H), 2.08 (s, 3H). UV−visible in 10% DMSO−DPBS (pH = 7.2) [λ_{max}, nm (ε, M^{-1} cm^{-1})]: 660 (2900), 457 (3600), 342 (10000), 285 (19000). IR data in solid phase (cm^{-1}): 3234 s, 3064 s, 2923 s, 2853 s, 1688 s, 1640 s, 1603 s, 1544 s, 1472 s, 1429 s, 1244 m, 1042 w, 780 w, 664 w, 580 w, 474 m. Λ_M, S m^2 M^{-1} in DMF at 25 °C: 83.

[Pt(Ph-tpy)(L^1)]Cl (**4**). Yield: 100 mg, 72%. Anal. Calcd for $C_{40}H_{44}ClN_7O_3PtS$ (**4**): C, 51.47; H, 4.75; N, 10.50. Found: C, 51.38; H, 4.92; N, 10.42. ESI-MS in MeOH: *m*/*z* 897.2973 ([M − Cl]$^+$, 100%). ^{1}H NMR (400 MHz, DMSO-d_6): δ 9.05 (m, 2H), 8.88 (m, 2H), 8.54 (d, 2H, *J* = 8 Hz), 8.21 (b, 3H), 7.95 (b, 2H), 7.70 (b, 6H), 6.41 (s, 1H), 6.35 (s, 1H), 4.30 (s, 1H), 4.13 (s, 1H), 4.12 (s, 2H), 3.08 (m, 1H), 2.99 (m, 2H), 2.82 (b, 1H), 2.58 (s, 1H), 2.15 (m, 2H), 2.04 (m, 2H), 1.61−1.52 (b, 12H). UV−visible in 10% DMSO−DPBS (pH = 7.2) [λ_{max}, nm (ε, M^{-1} cm^{-1})]: 398 (4400), 285 (19000), 257 (23000). IR data in the solid phase (cm^{-1}): 3400 s, 3334 s, 3236 s, 3214 s, 3062 m, 3000 m, 2939 m, 2888 m, 2856 m, 1690 s, 1649 s, 1610 s, 1531 m, 1480 m, 1412 m, 1245 m, 1103 w, 1032 w, 899 w, 774 s, 593 m, 572 m, 483 m, 462, m. Λ_M, S m^2 M^{-1} in DMF at 25 °C: 67.

[Pt(Ph-tpy)(L^2)]Cl (**5**). Yield: 97 mg, 79%. Anal. Calcd for $C_{34}H_{33}ClN_6O_2PtS$ (**5**): C, 49.79; H, 4.06; N, 10.25. Found: C, 49.58; H, 4.13; N, 10.11. ESI-MS in MeOH: *m*/*z* 784.1996 ([M − Cl]$^+$, 100%). ^{1}H NMR (400 MHz, DMSO-d_6): 9.12 (m, 2H) 9.03 (m, 2H), 8.87 (b, 2H), 8.55 (m, 2H), 8.19 (b, 3H), 7.89 (m, 2H), 7.69 (m, 3H), 6.41 (s, 1H), 6.35 (s, 1H), 4.65 (s, 1H), 4.18 (s, 1H), 4.11 (b, 2H), 3.11 (m, 1H), 2.80 (d, 1H, *J* = 4 Hz), 2.58 (b, 1H), 2.14 (m, 2H), 1.61−1.12 (b, 6H). UV−visible in 10% DMSO−DPBS (pH = 7.2) [λ_{max}, nm (ε, M^{-1} cm^{-1})]: 406 (5600), 330 (17000), 285 (27000), 258 (31000). IR data in the solid phase (cm^{-1}): 3472 s, 3352 s, 3247 s, 3129 s, 3069 s, 2485 m, 2415 m, 2173 m, 2076 m, 2025 m, 1673 s, 1653 s, 1605 s, 1541 m, 1477 m, 1415 m, 1244 m, 1029 w, 900 w, 768 s, 681 s, 590 w, 472 w, 438, m. Λ_M, S m^2 M^{-1} in DMF at 25 °C: 69.

[Pt(Ph-tpy)(L^3)]Cl (**6**). Yield: 88 mg, 92%. Anal. Calcd for $C_{26}H_{21}ClN_4OPt$ (**6**): C, 49.10; H, 3.33; N, 8.81. Found: C, 48.96; H, 3.49; N, 8.72. ESI-MS in MeOH: *m*/*z* 600.1364 ([M − Cl]$^+$, 100%). ^{1}H NMR (400 MHz, DMSO-d_6): δ 9.03 (m, 2H), 8.83 (m, 4H), 8.49 (m, 2H), 8.21 (b, 3H), 7.95 (m, 2H), 7.83 (m, 2H), 7.69 (m, 1H), 4.12 (d, 2H, *J* = 4 Hz), 1.90 (s, 3H). UV−visible in 10% DMSO−DPBS (pH = 7.2) [λ_{max}, nm (ε, M^{-1} cm^{-1})]: 397 (3670), 330 (10300), 285 (18400), 260 (23300). IR data in the solid phase (cm^{-1}): 3328 s, 3272 s, 3231 s, 3051 m, 3002 m, 2160 s, 2104 m, 2025 m, 1645 s, 1606 s, 1528 m, 1476 m, 1415 s, 1248 m, 1029 m, 906 w, 768 s, 681 m, 592 m, 494 m. Λ_M, S m^2 M^{-1} in DMF at 25 °C: 73.

Solubility. The complexes were sparingly soluble in MeOH, MeCN, and ethyl acetate. They were soluble in DMF and dimethyl sulfoxide (DMSO). They were insoluble in diethyl ether and hydrocarbon solvents.

Theoretical Calculations. The transitions in the visible region were obtained by performing linear-response time-dependent density functional theory (TDDFT) at the B3LYP/LanL2DZ level of theory using the *G09* suite programs.[33,40−43]

DNA Binding and Cleavage Experiments. ct-DNA (5 mL, 500 μM) was treated with complexes **1**−**6** (50 μM) in 10% DMSO−DPBS (pH = 7.2). The platinum contents in the isolated DNA in the dark and under photoirradiated conditions were evaluated by ICP-MS methods. The detailed procedures for DNA melting and viscosity experiments are provided in the Supporting Information.

SC pUC19 DNA (0.2 μg, 30 μM, 2686 base pairs) was preincubated for 1 h with complexes **1**−**6** (20 μM in 10% DMF−Tris-HCl buffer (50 mM), pH = 7.2, 37 °C) and then subjected to photoexposure using an argon−krypton mixed-gas ion laser of 647 nm for 1 h. The percentage of nicked-circular (NC) DNA was evaluated using gel electrophoresis with a UVITEC Gel Documentation System.[44] The DNA photocleavage measurements were also done in the presence of different additives such as ROS scavengers/quenchers (NaN_3, 4 mM; TEMP, 4 mM; DMSO, 8 μL; KI, 4 mM; catalase, 4 units; SOD, 4 units) using procedures that were reported earlier.[34]

MTT and DCFDA Assays. MTT, upon reduction by NAD(P)H-dependent cellular oxidoreductase enzymes present in the cytoplasm of metabolically active cells, forms formazan as a purple insoluble product. The amount of formazan estimated by a spectral method correlates with the number of live cells and provides a quantitative measurement of the cytotoxicity of the compound. The IC_{50} values were obtained from nonlinear regression using *GraphPad Prism 5*. About 8000 cells of BT474 (human breast carcinoma) and HBL-100 (normal breast epithelial human cells) were preincubated for 24 h in the dark with varying concentrations (50, 40, 30, 25, 20, 10, and 5 μM) of complexes **1**−**6**. Photoirradiation was done in a DPBS medium in visible light of 400−700 nm using a Luzchem photoreactor (model LZC-1, Ontario, Canada, 10 J cm^{-2}). Data were obtained as the average of three independent sets of experiments, all performed in triplicate for each concentration. DCFDA assay was done to quantify ROS on the oxidative production of fluorescent DCF (λ_{em} = 525 nm). BT474 cells (∼2 × 10^5 cells plated in duplicate) were incubated in the presence or absence of complexes **1**−**6** (concentration = IC_{50} values in light) for 24 h in the dark with or without photoirradiation in DPBS (400−700 nm, 1 h). Cells were trypsinized and treated with 1 μM DCFDA for ∼15 min, and the stained cells were determined by flow cytometry.

Annexin V-FITC/PI Assay. BT474 cells (∼2 × 10^5) were incubated (concentration = IC_{50} values in light) for 24 h followed by light treatment in DPBS (400−700 nm, 10 J cm^{-2}). Cells were further kept for 12 h post-treatment and then trypsinized. Annexin V-FITC (2 μL) and propidium iodide (PI; 1 μL) were then added to clear suspensions of cells in 500 μL of a 1X binding buffer and kept in the dark for 10 min. The percent cell population in each quadrant was estimated by FACS analysis. Experiments were performed in duplicate along with untreated controls for reference.

DOI: 10.1021/acs.inorgchem.6b00680
Inorg. Chem. XXXX, XXX, XXX−XXX

Table 1. Selected Physicochemical Data of Complexes 1−6

	1	2	3	4	5	6
λ_{abs}[a]/nm (ε/$M^{-1}cm^{-1}$)	640 (2700), 455 (3400)	642 (2900), 462 (3400)	660 (2900), 457 (3600)	398 (4400), 285 (19000)	406 (5600), 330 (17000)	397 (3700), 330 (10300)
λ_{emi}[b]/nm	635	635		640	639	640
$\Phi \times 10^5$	1.5	3.2		50	43	10
$\tau/\mu s$	0.015	0.018	<0.01	0.2	0.25	0.09
IR: ν_{N-H}[c]/cm^{-1}	3240, 3064	3229, 3063	3234, 3064	3214, 3062	3247, 3129	3272, 3231
IR: $\nu_{C=O}$[c]/cm^{-1}	1688, 1639	1687, 1643	1688, 1640	1690, 1649	1673, 1653	1645, 1606
CV	0.25	0.26	0.25			
E_f[d]/V [ΔE_p/mV]	−1.81 [95], −1.32 [75]	−1.82 [85], −1.30 [100]	−1.79 [80], −1.28 [105]	−1.76 [65], −1.20 [65]	−1.76 [80], −1.24 [85]	−1.76 [90], −1.24 [90]
Λ_M[e]/S m^2 mol^{-1}	65	70	83	67	69	73

[a]In 10% DMSO−DPBS (pH = 7.2). [b]In DCM at 298 K (excitation wavelength = 470 nm). The quantum yield was calculated using $[Ru(bpy)_3](PF_6)_2$ in MeCN as the standard (Φ = 0.062). [c]IR spectra recorded in the solid phase. [d]Peaks corresponding to cyclic voltamogramms of 1 mM sample in DMF−0.1 M TBAP. The potentials are recorded versus SCE (E_0 = 0.244 V), and values are reported relative to Fc/Fc^+ using ferrocene (E_f = 0.437 V) as the internal standard. $E_f = 0.5(E_{pa} + E_{pc})$. $\Delta E_p = (E_{pa} - E_{pc})$, where E_{pa} and E_{pc} are the anodic and cathodic peak potentials, respectively. Scan rate = 50 mV s^{-1}. [e]Molar conductivity in DMF.

Cell Cycle Analysis. Complexes **1**−**6** (concentration = IC_{50} values in light) were added to the BT474 cells (~2 × 10^5), incubated in the dark for 24 h, and photoirradiated in visible light (400−700 nm, 1 h). FACS analysis was done with samples (in duplicate) along with dark and untreated controls. The percentage of cells in each cell-cycle phase was obtained by data analysis using *WinMDI*, version 2.8.

Cellular Uptake from Platinum Estimation. To quantify the total platinum uptake, about 10^6 BT474 cells were seeded in 60 mm tissue culture dishes and treated with complexes **1**−**6** (50 μM) for 24 h. One identical plate was used to determine the protein content by Bradford assay. Similar experiments were performed with or without prior incubation of cells in the presence of biotin (100 μM) for 2 h. The samples were run using ICP-MS for the platinum content along with the standards (0, 100, 250, and 500 ppb fitted in a linear plot with a correlation of 0.91). The platinum content obtained in ppb units was then expressed as ng of Pt/μg of protein. All of the experiments were performed in triplicate and with untreated controls.

3. RESULTS AND DISCUSSION

Synthesis and General Properties. It was earlier observed that the metal-bound chloride in [(R-tpy)PtCl]Cl gets substituted by acetylide ligands, where R-tpy is a terpyridine (tpy) ligand with a pendant R group.[33] This synthetic strategy is useful to attach a cancer-targeting moiety to the metal-based photoinitiator. Biotinylated derivatives containing a free carboxylic group were coupled with propargylamine using anhydrous HOBt and EDCI to obtain the biotinylated acetylide ligands (Scheme S1 in the Supporting Information). The complexes were synthesized in ~85% yields by reacting the precursor [(R-tpy)PtCl]Cl (R = Fc for **1**−**3** and Ph for **4**−**6**) and ligands (HL^1 for **1** and **4**, HL^2 for **2** and **5**, and HL^3 for **3** and **6**) in DMF using a catalytic amount of CuI and excess triethylamine under a nitrogen atmosphere (Scheme S2 in the Supporting Information). The schematic drawings of **1**−**6** and the ligands used are shown in Figure 1. The purity of the complexes was checked by HPLC, ICP-MS, and CHN analysis (Figure S4 in the Supporting Information). Selected characterization data are given in Table 1. The ^{1}H NMR spectra of the complexes were recorded and assigned to the respective protons (Figures S5−S7 in the Supporting Information). All of the complexes showed peaks in the region 7.7−9.1 ppm, which were assignable to the aromatic protons of the terpyridyl moiety. For complexes **1**−**3**, two doublets at 5.4 and 4.8 ppm and a singlet at 4.2 ppm were observed, which is characteristic of the protons of the cyclopentadienyl rings of the metal-coordinated Fc-tpy ligand. The biotinylated complexes **1**, **2**, **4**, and **5** showed additional signals in the regions 6.3−8.2 ppm (for N−H protons) and 1.2−4.2 ppm (for aliphatic protons). In contrast, the control complexes **3** and **6** displayed only a singlet at 1.9 ppm corresponding to the CH_3 group protons. The ^{13}C and ^{195}Pt NMR spectra could not be recorded because of the low solubility of the complexes in deuterated DMSO. The molar conductance values of the complexes recorded in DMF at 25 °C were in the range of 65−83 S m^2 M^{-1}, suggesting their 1:1 electrolytic nature. Mass spectral analysis of dilute MeOH solutions of the samples displayed a single peak (respective m/z values for **1**−**6** are 1005.25, 892.16, 708.10, 897.29, 784.19, and 600.13) which is in accordance with that expected for the ionized $[M - Cl]^+$ species. The presence of platinum and the unipositive charge were evident from the isotopic distribution pattern (Figures S8−S13 in the Supporting Information).

The UV−visible spectra of complexes **1**−**6** (50 μM) were recorded in 10% DMSO−DPBS (pH = 7.2). Complexes **1**−**3** with the ferrocene unit showed strong absorption bands in the visible region having maxima at 650 and 460 nm with respective ε values of ~2900 and ~3500 M^{-1} cm^{-1} (Figures 2 and S14 in the Supporting Information). These bands are characteristic of the metal-bound Fc-tpy ligand.[33,45] The coordination to platinum metal is important for observing the band in the red-light region (~650 nm) because it lowers the energy gap (HOMO−LUMO) by extensive conjugation. In contrast, the uncoordinated ligand Fc-tpy displays only a shoulder at 480 nm (ε, 2070 M^{-1} cm^{-1}) under similar conditions, emphasizing the

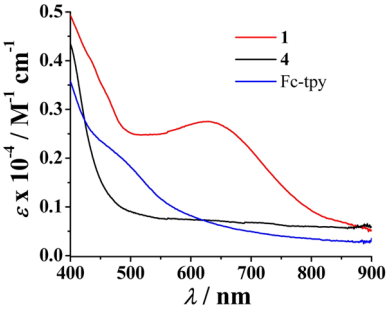

Figure 2. Visible absorption spectra of **1**, **4**, and Fc-tpy in 10% DMSO−DPBS (pH = 7.2).

DOI: 10.1021/acs.inorgchem.6b00680
Inorg. Chem. XXXX, XXX, XXX−XXX

need for metal coordination to observe the low-energy spectral band. An intense band within the spectral window of 600−800 nm is important in PDT considering greater tissue penetration of red light.[46] The Ph-tpy complexes **4**−**6** displayed absorption bands at ∼395 nm (ε, ∼ 4500 M^{-1} cm^{-1}). In the solid state at 298 K, the phenyl complexes **4**−**6** displayed broad emission bands in the red region (700−735 nm; Table 1 and Figure S15 in the Supporting Information). The ferrocene moiety acts as an efficient quencher of the ^{3}MLCT and ^{3}LC states, thereby resulting in no emission of complexes **1**−**3** at room temperature or at 77 K. This is in accordance with reductive quenching by the ferrocene unit reported for the Fc-tpy complexes.[47−49] The phenyl complexes **4**−**6** showed weak unstructured luminescence at ∼640 and 710 nm (Φ ∼ 0.0005 and τ ∼ 0.2 μs) in dichloromethane solutions. The ferrocenyl complexes **1** and **2** showed very weak luminescence at around 635 nm (Φ ∼ 0.3 × 10^{-4} and τ ∼ 0.015 μs). The complexes showed no significant luminescence in MeCN, DMSO, or DMF or in aqueous DMSO. The IR spectral signals were observed in the ranges 3000−3250 cm^{-1} for amide N−H stretch, 2850−2900 cm^{-1} for C≡C and C−H stretches, and 1540−1690 cm^{-1} for C═O, C═C, and C−N stretches (Figure S16 in the Supporting Information).[50] Out-of-plane N−H frequencies were observed at 700 cm^{-1}.

Electrochemical Studies. The redox properties of the ferrocene (Fc)-appended complexes **1**−**3** were studied using 1.0 mM solutions in DMF−0.1 M TBAP. The potentials versus SCE were corrected with reference to Fc/Fc^+ (E_f = 0.437 V). The Fc/Fc^+ couples appeared as an irreversible to quasi-reversible response near 0.25 V (Table 1 and Figure S17 in the Supporting Information).[51] The anodic response was found to undergo a positive shift of ∼90 mV compared to the free Fc-tpy ligand. This is attributed to the increasing inductive effect of the electron-withdrawing tpy on metal chelation. This also indicates stabilization of the Fe^{II} redox state of Fc-tpy on binding to Pt^{II}, which is difficult to chemically oxidize compared to free Fc-tpy and ferrocene. The irreversibility of the peaks may be due to electrode poisoning, adsorption, or instability of the Fc^+ moiety in the complex. A cyclic voltammetric (CV) study using ferrocene and a free Fc-tpy ligand with same electrode configuration gave expected reversible peaks, thus eliminating the possibility of electrode poisoning or surface adsorption processes (Figure S18a,b in the Supporting Information). To probe the stability of the oxidized species, we carried out chronoamperometric studies by setting the voltage at +0.4 V (vs Fc/Fc^+). The UV−visible spectra recorded after certain time intervals indicated the loss of Fc-centered bands at 480 and 590 nm, suggesting degradation of the oxidized species (S18c in the Supporting Information). All of the complexes exhibited cathodic responses near −1.3 and −1.8 V, which are attributed to two successive one-electron-reduction processes involving the tpy moiety. The reversible reduction of the coordinated tpy moiety is relatively unperturbed by the attached ferrocenyl or phenyl moiety. The free ligands Ph-tpy or Fc-tpy did not show such reduction (Figure S18d in the Supporting Information). The biotinylated ligands were also redox-inactive within the voltage window. The phenyl analogues **4**−**6** showed no oxidation peaks due to the lack of a Fc moiety. The results suggest that the ferrocenyl complexes could undergo oxidation upon photoexposure, with their phenyl analogues being inactive.

TDDFT Calculations. We attempted to rationalize the strong absorptions in the visible region and the photophysical properties of the Fc-tpy complexes **1**−**3** with theoretical studies using the B3LYP/LanL2DZ level of theory with the *Gaussian G09* suite of programs.[40−43] The coordinates for the basic structures of **1**−**3** were taken from the crystal structure of [Pt(Fc-tpy)Cl]Cl and then modified as required by adding the acetylide fragments. These coordinates were utilized to obtain the respective energy-minimized structures by DFT methods (Figure S19 and Table S1 in the Supporting Information). In the optimized structure of complex **1**, the ferrocenyl ring and the aliphatic chain containing the biotin moiety adopted close configurations because of the flexibility of the long alkyl chains. Interestingly, a chemically significant N−H···π interaction was observed in the optimized structure of **1**. The distance of hydrogen of the amide group of the biotin unit from the unsubstituted Cp ring of the Fc unit was 2.53 Å, thereby signifying the presence of weak interactions, which stabilized the molecule in such a configuration. To further understand the localizations and contributions of the molecular orbitals responsible for such transitions, we performed TDDFT on these energy-minimized ground-state geometries. Selected transitions within the 400−900 nm range along with their oscillator strengths (f) are listed in Table S2 in the Supporting Information. The highest probable transition was at 592.04 nm for **1** (f = 0.0270), 592.25 nm for **2** (f = 0.0276), and 590.99 nm for **3** (f = 0.0302). This transition was assignable to the ligand moiety (Fc-tpy) to platinum(II) metal charge transfer (LMCT; ∼40%), viz., from the d orbitals of Fe of Fc (HOMO−3 for **1**, HOMO−1 for **2**, and HOMO for **3**) to the π orbitals of Pt-tpy (LUMO), and intraligand charge transfer (ILCT; ∼45%), viz., from the d orbitals of Fe in Fc (HOMO−4 for **1**, HOMO−3 for **2**, and HOMO−1 for **3**) to the π orbitals of Cp rings (LUMO+6; Figures 3 and S20 and S21 in the Supporting Information). The absence of such transitions in free Fc-tpy suggests the important contribution of the low-lying orbitals from the metal-coordinated ligands for the realization of strong absorptions in the low-energy visible spectral region. Computations also revealed strong absorptions at 515 and 465 nm for all of the complexes with respective f values of ca. 0.02

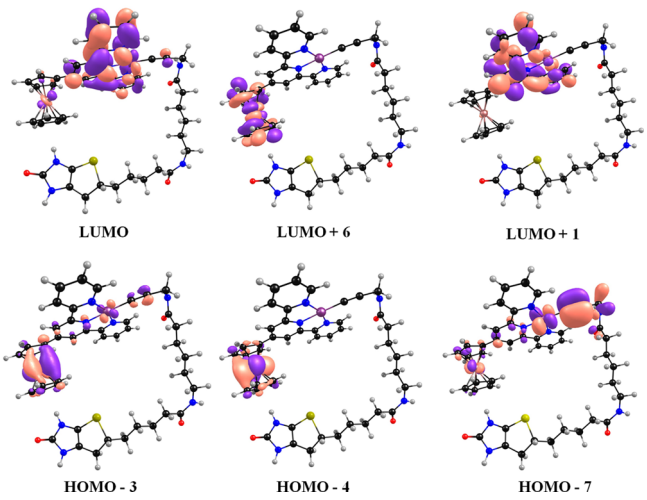

Figure 3. Frontier molecular orbitals of complex **1** involved in transitions in the red light region as obtained from TDDFT calculations using the B3LYP/LanL2DZ level of theory. Color code: purple, platinum; red, oxygen; blue, nitrogen; black, carbon; yellow, sulfur; gray, hydrogen. The orbitals are drawn using a contour value of 0.03.

DOI: 10.1021/acs.inorgchem.6b00680
Inorg. Chem. XXXX, XXX, XXX−XXX

and 0.01. Interestingly, these transitions were characterized by charge transfer (L′MCT and IL′CT; ∼90%) involving the triple-bonded ligands (HOMO−9 and HOMO−7 for **1**, HOMO−5 and HOMO−7 for **2**, and HOMO−2 and HOMO−4 for **3**) and Fc-tpy-Pt (LUMO and LUMO+1; Figure 3 and S18 and S19 in the Supporting Information). The comparatively low energy gap of transitions (ΔE = −1.5 eV) compared to free ferrocene (ΔE = −5.5 eV) or Fc-tpy (−4.2 eV) makes them better photoinitiators capable of responding to longer-wavelength irradiation. Additionally, it was observed that the orbitals of the ferrocenyl (Fc) moiety and that of Pt−≡−L′ comprise mainly antibonding interactions and, hence, are dissociative in nature. This suggests probable loss of the ferrocenyl unit, which also triggers Pt−C(acetylide) bond dissociation in the excited states of these photodegradation-prone molecules.[52,53]

Mechanism of Photodegradation. The stability of the complexes was studied in different solvents in the presence of additives under photoirradiation and in dark conditions. The solvents, additives, and extensive conjugation in the complexes were found to have a profound impact on the photodegradation processes of ferrocenyl complexes. Complexes **1**−**6** (50 μM) were found to be stable in 10% DMSO−DPBS (pH = 7.2) or in DMSO for 48 h in the dark. However, the Fc-tpy complexes **1**−**3** degraded upon photoexposure to broad-band visible light of 400−700 nm (Luzchem photoreactor, 10 J cm^{-2}) or to red laser light of 647 nm (50 mW). The mechanistic pathway and photoproducts were investigated by UV−visible absorption, ^{1}H NMR, and ESI-MS spectral methods. They exhibited solvent-dependent changes in the absorption spectra when monitored as a function of the photoirradiation time. The complexes upon photoirradiation in 10% DMSO−DPBS (50 μM, pH = 7.2) showed a gradual decrease of the intensity of the absorption at ∼650 and 460 nm after 1 h of photoexposure time (Figure S22 in the Supporting Information). In pure DMSO or DMF solvent, the irradiated complexes showed a red shift of the band from 580 to 640 nm with a large increment in the ε value (from 6770 to 21460 M^{-1} cm^{-1}) upon just 30 s of light exposure (Figure S23 in the Supporting Information). The band gradually flattened upon continuous photolysis, and the green solution turned initially to sky blue, then to deep blue, and finally black (Figure S23d in the Supporting Information). This rapid spectral change was attributed to solvent charge-transfer transitions in the oxidized Fc moiety, which are favored in electron-acceptor solvents like DMSO or DMF.[54] A similar rapid loss of the visible spectral band was visible upon the addition of ceric ammonium nitrate (CAN) as an oxidizing agent, turning the solution to yellow (the color of excess CAN), indicating the involvement of a photooxidative process (Figure S23 in the Supporting Information). The addition of 1,10-phenanthroline (phen) to the 30 min photoirradiated solution of the complex gave a red solution showing two new bands at 520 and 430 nm, which are assignable to a tris-phen complex of iron(II) (Figure S24 in the Supporting Information).[55] Mass analysis of these samples showed the presence of a peak at m/z 298.18, confirming the formation of a Fe^{II}-phen species (Figure S25 in the Supporting Information). Similar absorption bands at 520 and 430 nm appeared when a solution of ferric chloride was treated with phen, turning the solution red (Figure S26 in the Supporting Information). Mass spectral analysis of these diluted samples also exhibited a prominent peak at m/z 298.18, thereby indicating the formation of a tris-phen complex of iron(II). This experiment confirmed that the iron(III) from the excited state can be stabilized in the lower oxidation state of 2+ in the presence of π-acidic ligands like phen. We can thus infer that metal chelators like phen can leach out iron from the complex in its photoexcited state and form stable binary species. The effect of the addition of excess glutathione (GSH) was explored because GSH is highly abundant in cancer cells (∼15 mM). When the complexes were photoirradiated in the presence of GSH (15 mM in 10% DMSO−DPBS), the absorption bands at longer wavelengths showed instant decay and the solution turned yellow, giving two new bands at 575 and 580 nm (Figure S27 in the Supporting Information). The mass spectral pattern of these solutions did not show the formation of any species of discrete composition.

It is apparent from the ^{1}H NMR analysis in DMSO-d_6 that the complexes released the unsubstituted cyclopentadienyl ring (Cp, C_5H_5) of the ferrocenyl moiety upon photoirradiation, with new peaks appearing as a multiplet at 6.5−6.4 ppm and a singlet at 2.7 ppm (Figures 4 and S28 and S29 in the Supporting Information). To further support the leaching out of the Cp ring,[56,57] we performed a control photolysis experiment with 1,1′-bis(diphenylphosphino)ferrocene in UVA light of 395 nm. In this Fc derivative, the substituted Cp ring has high molecular weight and, hence, the photorelease can be detected by mass spectra. After 5 h of photoexposure, the faint yellow color of the DMSO solution intensified. NMR and mass spectral evidence pointed out the release of cyclopenta-1,3-dien-1-yldiphenylphosphine oxide (Figures S30 and S31 in the Supporting Information). The phosphorus in the released species was found to be oxidized, which confirms the generation of ROS (the m/z value for the protonated species is 267.09). It is a favorable argument to conclude that complexes **1**−**3** followed an analogous mechanism upon photoexposure at longer wavelengths and shorter irradiation times, which is due to the presence of extensive conjugation and metal coordination. Another interesting observation from the NMR studies was the release of the triple-bonded ligands upon prolonged photoexposure of the complex (Figures 4 and S28 and S29 in the Supporting Information). The peak appearing at 2.2 ppm upon light exposure of complex **3** is assignable to the acetylenic proton of C≡CH, indicating dissociation of the Pt−acetylide bond. These samples were then diluted with HPLC-grade MeOH and subjected to mass

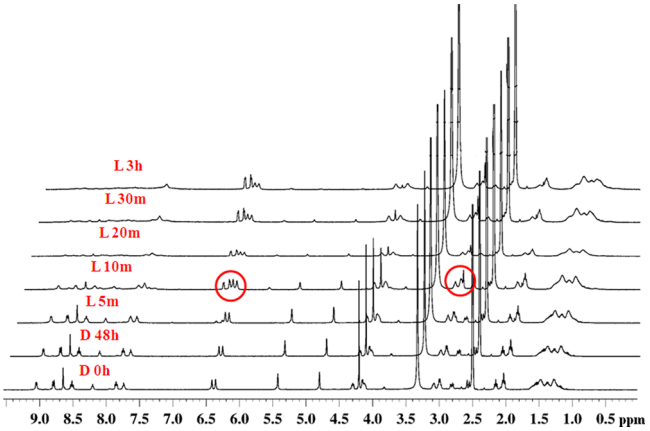

Figure 4. Time-dependent photoinduced (400−700 nm) ^{1}H NMR spectral changes of complex **1** (5 mM in DMSO-d_6) as indicated in the figure (L = light of 400−700 nm, 10 J cm^{-2}, D = dark, and m = photoexposure time in min).

DOI: 10.1021/acs.inorgchem.6b00680
Inorg. Chem. XXXX, XXX, XXX−XXX

analysis. The respective m/z 395.25 and 282.13 [assigned to free ligands, $(M + H)^+$] proved cleavage of the Pt−C(acetylide) bond in light (Figures S32a,b in the Supporting Information). The photoinduced detachment of the biotin ligand is of interest because this provides an effective way of delivering the complexes with the help of biotin receptors and then releasing the active phototoxin with the help of light. A peak of m/z 485.7 corresponding to $[Pt(tpy)Cl]^+$ was observed in the mass spectrum of the photodegraded complex **3** (Figure S32c in the Supporting Information). All of the experiments when repeated in darkness showed unaltered spectra, implying the importance of light activation for achieving degradation of the complex. In summary, these results altogether suggest a photoredox process to be operative in the light-promoted degradation of complexes **1**−**3** having a redox-active extensively conjugated Fc-tpy moiety (Scheme S3 in the Supporting Information). In contrast, the phenyl analogues showed significant photostability.

Platinum Estimation. Photorelease of the biotinylated ligands led to the formation of an active platinum(II) species that can bind to ct-DNA. To explore such a possibility, we treated two identical sets of ct-DNA (5 mL, 500 μM) with complexes **1**−**3** (50 μM). One such set was photoirradiated in visible light (400−700 nm) for 1 h, while the other was kept in darkness. The DNA was then precipitated with an excess of cold ethanol and isolated to measure the amount of platinum covalently bound to DNA. Complexes **1**−**3** showed prominent enhancement (∼500 pg of Pt/μg of DNA) in DNA-bound platinum amounts only after irradiation of the samples (Table S3 in the Supporting Information). The phenyl analogues, however, did not show any significant increase of platinated DNA in darkness or upon exposure to light.

DNA Binding and Cleavage Studies. The DNA melting experiments were done to explore the effect of the complexes (10 μM) on the melting temperatures (T_m) of ct-DNA (100 μM; Figure S33a in the Supporting Information). Intercalation of the planar aromatic molecules between the DNA base pairs stabilizes the duplex DNA, which is reflected in an increase of the melting temperature (ΔT_m). The ΔT_m values of ∼0.5 °C for **1**−**3** indicate the lack of DNA intercalation of the Fc-tpy complexes. In contrast, the phenyl analogues **4**−**6** gave a ΔT_m value of ∼5 °C, suggesting an intercalative mode of their binding to ct-DNA. EB as a DNA intercalator gave a ΔT_m value of 11 °C under similar conditions. The viscosity of ct-DNA is known to be significantly altered in the presence of DNA intercalators or groove binders. Viscometric data suggested intercalative properties of the Ph-tpy complexes **4**−**6**. It was also observed from the viscosity plot of $(\eta/\eta_0)^{1/3}$ versus [complex]/[DNA], where η and η_0 are the viscosities of DNA in the presence and absence of the complex, that the Fc-tpy complexes caused only minor changes in the viscosity, indicating their inability to bind to ct-DNA in an intercalative manner (Figure S33b in the Supporting Information). Intercalation within the base pairs also results in an enhancement of the emission intensity due to trapping of the molecule in the hydrophobic DNA core. Only the phenyl complexes **4**−**6** showed notable enhancement of the luminescence intensity in DNA-buffer solutions, which further demonstrated the DNA intercalating ability of Pt^{II}(Ph-tpy) (Figure S34 in the Supporting Information).[58]

The possibility of any ROS generation upon photodegradation of the complexes was explored from the DNA photocleavage experiments using complexes **1**−**3** and different additives.[59] The photocleavage of SC pUC19 DNA (0.2 μg, 30 μM, 2686 base pairs) was studied using red light of 647 nm (Figure 5). This wavelength was chosen considering the 640

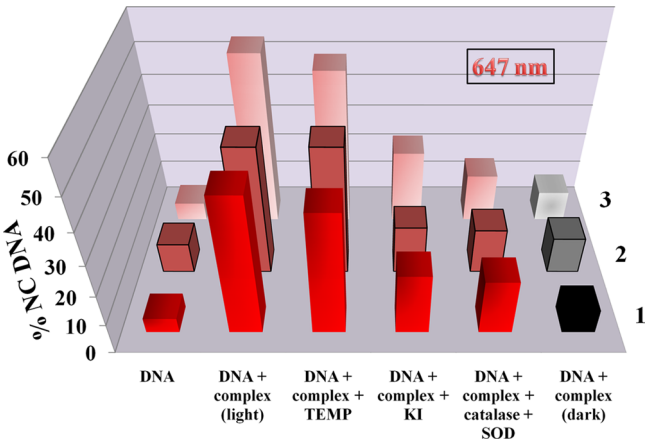

Figure 5. Photoinduced cleavage of pUC19 DNA in the presence of Fc-tpy complexes **1**−**3** (20 μM in 10% DMF buffer) in light (red bars, Ar−Kr continuous-wave laser source, 647 nm, 50 mW) and dark (black bars) as shown in the figure. Different additives added: NaN_3 or TEMP (4 mM), KI (4 mM), or DMSO (8 μL), catalase, and SOD (4 units).

nm absorption maxima of the photoactive Fc-tpy complexes **1**−**3**. The complexes (20 μM in 10% DMF buffer, pH = 7.2) showed photoinduced SC DNA cleavage, resulting in the formation of ∼50% NC form. The presence of singlet oxygen quenchers like TEMP and NaN_3 (4 mM) failed to inhibit DNA cleavage, thus excluding the formation of any singlet oxygen ($^1O_2$) as the ROS. The formation of NC DNA was, however, reduced to ∼25% in the presence of hydroxyl radical scavengers, viz., KI (4 mM) and DMSO (8 μL). The DNA photocleavage activity was also decreased (∼20% NC) in the presence of SOD (4 units) and catalase (4 units), suggesting the formation of hydroxyl radicals ($^{\bullet}$OH) via superoxide and hydrogen peroxide as the ROS.

Cell Viability Studies. Photodegradation of the Fc-tpy complexes, leading to the generation of radical species prompted us to investigate the antiproliferative properties of the complexes in cancer cells in light (400−700 nm, 10 J cm^{-2}) and in the dark. With the complexes having pendant biotin units, we selected the biotin-receptor positive cells, viz., human breast carcinoma cancer cells (BT474), to assess the cellular activity. Human normal breast epithelial cells (HBL-100) were taken as the reference to validate the selective uptake of these complexes. Colorimetric MTT assay, based on an estimation of the resulting purple formazan by spectral methods, was used to determine the IC_{50} values of the complexes (Figures 6 and S35 in the Supporting Information). The results were compared with those known for related photoactive platinum(II) and tpy−metal complexes (Table 2).[33a,34,35,60,61] Complex **1** showed photoinduced cytotoxicity in BT474 cells, giving an IC_{50} value of ∼7 μM in visible light (400−700 nm), while remaining essentially nontoxic in the dark (IC_{50}: >50 μM). Complexes **2** and **3** gave IC_{50} values of ∼16 μM upon light exposure. This implies that the presence of a spacer moiety in complex **1** resulted in better cellular uptake, which can be correlated with its better cellular toxicity. Upon comparison, it was observed that complex **1** exhibited comparable photocytotoxicity with less dark toxicity than the previously reported complexes. However, the other complexes did not have any

DOI: 10.1021/acs.inorgchem.6b00680
Inorg. Chem. XXXX, XXX, XXX−XXX

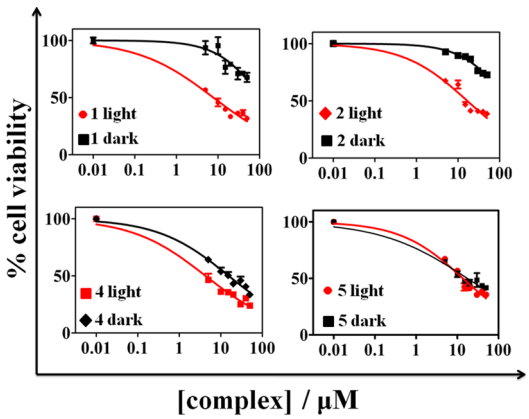

Figure 6. Cell viability plots in BT474 cells preexposed to biotinylated complexes **1**, **2**, **4**, and **5** for 24 h in the dark followed by either photoirradiation (10 J cm^{-2}, 400−700 nm) or darkness.

tumor-targeting moieties attached to them, which rendered them unspecific in action. In contrast, the phenyl analogues displayed high dark toxicity, as is known for several tpy complexes of platinum(II) possibly because of their better DNA intercalating properties, as predicted from the DNA melting and viscosity data.[33b,62−65] Complex **4** gave an IC_{50} value of 4 μM in light, which is comparable to that of cisplatin. The nonbiotinylated control complex **6** showed ∼5-fold lower toxicity compared to **4** with an IC_{50} value of 24 μM. Interestingly, the biotin complexes **1**, **2**, **4**, and **5** showed low cytotoxicity in the normal cell line HBL-100 (IC_{50}: ∼40 μM), while the control complexes **3** and **6**, lacking the biotin moiety, showed toxicity similar to that observed in the cancer cells (IC_{50}: ∼25 μM). The MTT assay data highlight the importance of the biotin moiety toward achieving selective therapeutic activity in the cancer cells.

Biotinylated compounds are well-known for their increased cellular uptake via streptavidin−avidin receptors that are overexpressed in cancer cells.[16−18] Thus, we hypothesized that the biotin complexes resulted in better cytotoxicity because of enhanced cellular uptake compared to their control counterparts. To justify our argument, we further carried out cellular uptake studies by a quantified estimation of the total platinum uptake within the cells. The results given in Table 3 show the highest cellular platinum amount (∼10−11 ng of Pt/μg of protein) of complexes **1** and **4**. Complexes **3** and **6** showed lower cellular uptake (∼2.8 and 7.5 ng of Pt/μg of protein, respectively). It was also observed that prior treatment of the cells with biotin (100 μM) for 2 h suppressed cellular uptake of the biotinylated complexes **1**, **2**, **4**, and **5**. The uptake of **1** (11 ng of Pt/μg of protein) was reduced by presaturation of biotin receptors to 2.5 ng of Pt/μg of protein. Similar results were also obtained for complex **4**, which showed reduced uptake to half upon prior treatment of the cells with biotin. In contrast, the nonbiotinylated complexes **3** and **6** showed similar cellular uptake values in the absence or presence of biotin. The complexes did not react with the externally added biotin, as evidenced from the unaltered mass and NMR spectra, and this ruled out any possibility of interaction of the complex with biotin, which may lead to the lowering of cellular uptake. It is thus concluded that the biotin-receptor-mediated uptake of the complexes was responsible for their potent toxicity selectively in the cancer cells.

Table 3. Cellular Uptake of Complexes in BT474 Cells Expressed as ng of Pt/μg of Protein

complex	without biotin[a]	with biotin[b]
untreated	0.0	0.0
1	11.15 ± 0.82	2.48 ± 0.13
2	3.83 ± 0.20	1.80 ± 0.15
3	2.77 ± 0.52	2.14 ± 0.15
4	10.65 ± 1.06	5.42 ± 0.57
5	8.65 ± 1.17	4.67 ± 0.33
6	7.56 ± 0.85	6.91 ± 0.64

[a]BT474 cells treated with the complexes (50 μM) for 12 h in the dark. [b]Cells preincubated with biotin (100 μM) for 2 h and then treated with the complexes (50 μM) for 12 h in the dark. The platinum content estimated by the ICP-MS method.

ROS and Cellular Apoptosis. Light-promoted generation of ROS is an essential feature of PDT agents. Cellular ROS production by complexes **1**−**3** was examined by 2,7-dichlorofluorescein diacetate (DCFH-DA) assay (Figure 7). This cell-permeant nonfluorescent dye gets oxidized by cellular ROS to produce 2,7-dichlorofluorescein (DCF), which emits at 525 nm (λ_{exc} = 488 nm). The emission intensity of DCF was quantified by using FACS techniques, and it gave an estimate to the amount of ROS generated within the cells. Complexes **1**−**3** showed DCF formation (mean DCF intensity ∼3000 au) in BT474 cells only upon photoexposure to light of 400−700 nm but not in the dark (mean DCF intensity ∼900 au) (Figure

Table 2. Photocytotoxicity[a] of 1−6 As Determined from MTT Assay along with Selected Metal Complexes[b] for Comparison

	BT474		HBL-100	
complex	IC_{50}[c](light) (μM)	IC_{50}[d](dark) (μM)	IC_{50}[c](light) (μM)	IC_{50}[d] (dark) (μM)
1	7.7 ± 2.5	>50	45.2 ± 5.2	>50
2	16.7 ± 3.4	>50	42.6 ± 4.6	>50
3	16.9 ± 3.8	>50	24.5 ± 3.5	>50
4	4.3 ± 2.7	15.5 ± 3.1	20.2 ± 2.2	27.3 ± 5.4
5	13.7 ± 3.4	17.5 ± 5.2	28.5 ± 5.0	30 ± 4.3
6	20.7 ± 5.5	24.1 ± 4.2	22.4 ± 4.3	29.5 ± 4.2
HL^1	>50	>50	>50	>50
cisplatin		4.4 ± 2.3		15.6 ± 5.2

[a]The IC_{50} values (μM) obtained from MTT assay in BT474 and HBL-100 cells pretreated with complexes in the dark for 24 h, either followed by light exposure (400−700 nm, 10 J cm^{-2}) or kept in the dark. [b]The IC_{50} values (μM) in HaCaT cells of [Pt(Fc-tpy)Cl]Cl,[33a] [Pt(pap)(an-cat)],[34] $[Pt(NH_3)_2(cur)]NO_3$,[35] and $[VO(Fc\text{-}tpy)(py\text{-}acac)]ClO_4$[60] (in MCF-7 cells) and platinum(IV) diazido[61] are 12.2 (±0.5), 4.4 (±0.2), 13 (±4), 2.1 (±0.3), and 19.5 (±6.1) in visible light and 74.8 (±1.1), 43.5 (±0.8), >200, 38.5 (±1.1), and 70.2 (±6.1) in the dark, respectively. [c]In light of 400−700 nm (exposure time of 1 h). [d]In the dark.

DOI: 10.1021/acs.inorgchem.6b00680
Inorg. Chem. XXXX, XXX, XXX−XXX

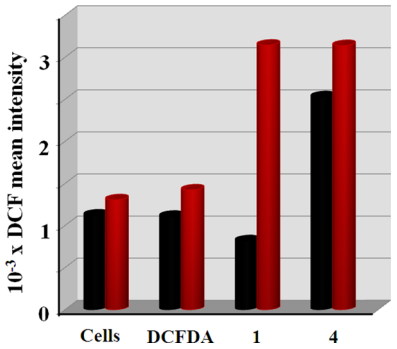

Figure 7. DCFH-DA assay showing generation of ROS in BT474 cells treated with complexes **1** and **4** for 24 h in the dark and exposed to light (red cylinders) or in the dark (black cylinders). The *y* axis denotes the mean DCF intensity (in arbitrary units) obtained with the cells alone/cells + DCFDA/cells + complexes + DCFH-DA (light, 400−700 nm, 10 J cm^{-2}, or in the dark).

S36a in the Supporting Information). In contrast, complexes **4**−**6** showed ROS generation (mean DCF intensity ∼2500 au) in both dark and light conditions because of their dark toxicity (Figure S36b in the Supporting Information).

The selective uptake of annexin V-FITC and PI divides the total cell population into four quadrants. PI stains the necrotic cells (upper left), annexin V-FITC stains the early apoptotic cells (lower right), late apoptotic cells uptake both dyes (upper right), and live cells are impermeable to both dyes (lower left). BT474 was pretreated with the complexes for 24 h, exposed to light for 1 h, and then subjected to annexin V-FITC/PI assay after a 12 h recuperation period (Figures 8 and S37 in the Supporting Information). Complexes **1**−**3** triggered the respective 65, 50, and 46% of early apoptosis upon light (400−700 nm) exposure. The observed early apoptotic cell population in the dark was 26% for **1**, 12% for **2**, and 22% for **3**, indicating the importance of light exposure to observe apoptotic cell death. Complexes **4**−**6** were almost equally active in the dark and light in the absence of any PDT effect, resulting in 80, 75, and 70% early apoptosis, respectively. The cell cycle profiling assay in BT474 cells, based on the amount of DNA stained by PI, quantified the sub-G1 DNA content. The Fc-tpy complexes **1**−**3** showed substantial sub-G1 arrest (∼30%) only upon photoirradiation with visible light (400−700 nm), while resulting in only ∼15% cell death in darkness. The Ph-tpy complexes **4**−**6** showed almost equal sub-G1 population (∼25−65%) in both dark and light conditions (Figure S38 in the Supporting Information).

4. CONCLUSIONS

Biotinylated platinum(II) complexes of the Fc-tpy ligand show the PDT effect in visible light and specific accumulation into the cancer cells over the normal cells. The Ph-tpy complexes, in contrast, do not show any apparent PDT effect. In addition, the Ph-tpy complexes show significant cellular toxicity in the dark. The Fc-tpy ligand alone is inactive in visible light, while the same upon binding to platinum(II) displays photoinduced cytotoxicity. The Fc-tpy complexes **1**−**3** were found to release biotinylated ligands in red light (647 nm, 50 mW), and this has possibly led to photoinitiated covalent DNA binding by an active platinum species. This is significant because premature activation of platinum(II) drugs like cisplatin and its analogues leads to side effects, and a spatially controlled release of the active species is desired. Furthermore, the release of the

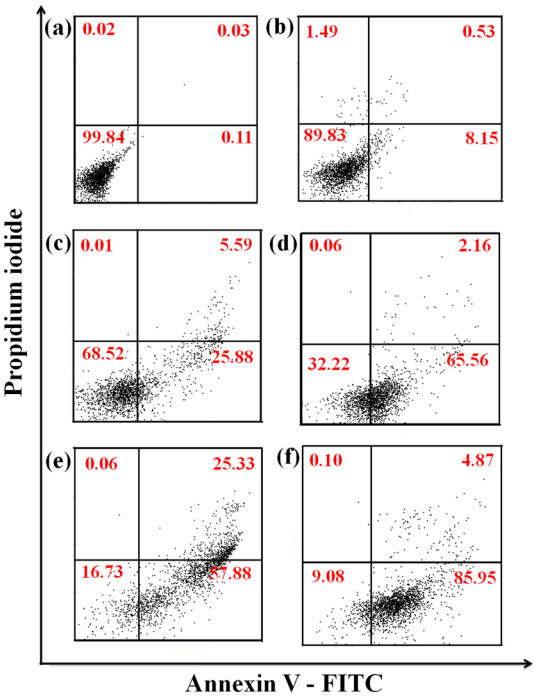

Figure 8. Annexin V-FITC/PI assay showing percent cell population of BT474 cells pretreated with the complexes (concentration = IC_{50} values in light) for 24 h in the dark: cells alone (a); cells + PI + annexin (b); complex **1** in the dark (c) and upon photoexposure (d); complex **4** in the dark (e) and upon photoexposure (f). Quadrants: lower left, live cells; lower right, early apoptosis; upper right, late apoptosis; upper left, dead cells.

biotinylated ligand upon photoactivation leads to the delivery of the phototoxin selectively into the cancer cells. Complex **1** showed potent light-mediated anticancer effects selectively in the cancer cells, giving a IC_{50} value of ∼7 μM. The high toxicity is attributed to the synergistic cytotoxic effects of the photoreleased active platinum species and ROS. The phenyl counterpart **4** paralleled the behavior of cisplatin under similar conditions, giving a IC_{50} value of 4 μM. The reduced activity of the nonbiotinylated counterparts and the reduced cellular uptake of the complexes in the presence of externally added biotin exemplify the important role biotin plays in achieving selective uptake of the complexes in the cancer cells. While the Fc-tpy complexes **1** and **2** define dual-action photochemotherapeutic agents, their phenyl analogues **4** and **5** act as cancer-cell-selective chemotherapeutic agents.

■ ASSOCIATED CONTENT

Supporting Information

The Supporting Information is available free of charge on the ACS Publications website at DOI: 10.1021/acs.inorgchem.6b00680.

Details of the experimental methods and measurements, reaction schemes (Schemes S1 and S2), mechanistic aspect (Scheme S3), NMR (Figures S1, S2, and S5−S7), ESI-MS (Figures S3 and S8−S13), HPLC chromatograms (Figure S4), UV−visible data (Figure S14), emission data (Figure S15), IR spectra (Figure S16), cyclic voltammograms (Figures S17 and S18), optimized structure and frontier molecular orbitals (Figures S19−S21), photostability (Figures S22−S32), DNA melting and viscosity (Figure S33), luminescence (Figure S34),

DOI: 10.1021/acs.inorgchem.6b00680
Inorg. Chem. XXXX, XXX, XXX−XXX

MTT assay (Figure S35), FACS analysis (Figures S36–38), Cartesian coordinates and electronic transitions in the complexes (Tables S1 and S2), and platinum content in ct-DNA (Table S3) (PDF)

AUTHOR INFORMATION

Corresponding Authors

*E-mail: paturu@mrdg.iisc.ernet.in. Tel.: +91-80-22932688. Fax: +91-80-3600999.

*E-mail: arc@ipc.iisc.ernet.in. Tel.: +91-80-22932533. Fax: +91-80-23600683.

Author Contributions

The manuscript was written through contributions of all authors. All authors have given approval to the final version of the manuscript.

Notes

The authors declare no competing financial interest.

ACKNOWLEDGMENTS

We thank the Department of Science and Technology (DST), Government of India (GOI), for financial support (Grants SR/S5/MBD-02/2007 and EMR/2015/000742). A.R.C. thanks the DST for a J. C. Bose national fellowship and the Alexander von Humboldt Foundation, Germany, for donation of an electrochemical system. K.M is a recipient of a BMS fellowship. A.S. is a recipient of a Dr. D. S. Kothari postdoctoral fellowship of UGC. P.K. received financial support from the Department of Biotechnology, GOI. We are thankful to Ms. Urvashi for FACS analysis. We thank Dr. R. Chakrabarti, Centre for Earth Sciences, of our institute for the ICP-MS facility. We thank Ms. Sharada for her help in recording solid-state emission.

REFERENCES

(1) (a) Farrer, N. J.; Salassa, L.; Sadler, P. J. *Dalton Trans.* **2009**, 10690–10701. (b) Shirasu, N.; Nam, S. O.; Kuroki, M. *Anticancer Res.* **2013**, *33*, 2823–2832.

(2) Velema, W. A.; Szymanski, W.; Feringa, B. L. *J. Am. Chem. Soc.* **2014**, *136*, 2178–2191.

(3) Craig, R. A.; McCoy, C. P.; Gorman, S. P.; Jones, D. S. *Expert Opin. Drug Delivery* **2015**, *12*, 85–101.

(4) Garner, R. N.; Gallucci, J. C.; Dunbar, K. R.; Turro, C. *Inorg. Chem.* **2011**, *50*, 9213–9215.

(5) Chen, H.; Tian, J.; He, W.; Guo, Z. *J. Am. Chem. Soc.* **2015**, *137*, 1539–1547.

(6) Renfrew, A. K. *Metallomics* **2014**, *6*, 1324–1335.

(7) Pattni, B. S.; Chupin, V. V.; Torchilin, V. P. *Chem. Rev.* **2015**, *115*, 10938–10966.

(8) Dhar, S.; Kolishetti, N.; Lippard, S. J.; Farokhzad, O. C. *Proc. Natl. Acad. Sci. U. S. A.* **2011**, *108*, 1850–1855.

(9) Olivo, M.; Bhuvaneswari, R.; Lucky, S. S.; Dendukuri, N.; Thong, P. S.-P. *Pharmaceuticals* **2010**, *3*, 1507–1529.

(10) (a) Basu, U.; Pant, I.; Hussain, A.; Kondaiah, P.; Chakravarty, A. R. *Inorg. Chem.* **2015**, *54*, 3748–3758. (b) Basu, U.; Khan, I.; Hussain, A.; Gole, B.; Kondaiah, P.; Chakravarty, A. R. *Inorg. Chem.* **2014**, *53*, 2152–2162.

(11) Leonidova, A.; Foerster, C.; Zarschler, K.; Schubert, M.; Pietzsch, H.-J.; Steinbach, J.; Bergmann, R.; Metzler-Nolte, N.; Stephan, H.; Gasser, G. *Chem. Sci.* **2015**, *6*, 5601–5616.

(12) (a) Zheng, Y.-R.; Suntharalingam, K.; Johnstone, T. C.; Yoo, H.; Lin, W.; Brooks, J. G.; Lippard, S. J. *J. Am. Chem. Soc.* **2014**, *136*, 8790–8798. (b) Scott, A. M.; Wolchok, J. D.; Old, L. J. *Nat. Rev. Cancer* **2012**, *12*, 278–287.

(13) Chen, S.; Zhao, X.; Chen, J.; Chen, J.; Kuznetsova, L.; Wong, S. S.; Ojima, I. *Bioconjugate Chem.* **2010**, *21*, 979–987.

(14) Bareford, L. M.; Swaan, P. W. *Adv. Drug Delivery Rev.* **2007**, *59*, 748–758.

(15) Ojima, I.; Zuniga, E. S.; Berger, W. T.; Seitz, J. D. *Future Med. Chem.* **2012**, *4*, 33–50.

(16) Tripodo, G.; Mandracchia, D.; Collina, S.; Rui, M.; Rossi, D. *Med. Chem.* **2014**, *S*, 1–8.

(17) Vadlapudi, A. D.; Vadlapatla, R. K.; Pal, D.; Mitra, A. K. *AAPS J.* **2012**, *14*, 832–842.

(18) Vadlapudi, A. D.; Vadlapatla, R. K.; Mitra, A. K. *Curr. Drug Targets* **2012**, *13*, 994–1003.

(19) Saha, S.; Majumdar, R.; Hussain, A.; Dighe, R. R.; Chakravarty, A. R. *Philos. Trans. R. Soc., A* **2013**, *371*, 20120190.

(20) Sun, Q.; Qian, J.; Tian, H.; Duan, L.; Zhang, W. *Chem. Commun.* **2014**, *50*, 8518–8521.

(21) Vineberg, J. G.; Wang, T.; Zuniga, E. S.; Ojima, I. *J. Med. Chem.* **2015**, *58*, 2406–2416.

(22) Vineberg, J. G.; Zuniga, E. S.; Kamath, A.; Chen, Y.-J.; Seitz, J. D.; Ojima, I. *J. Med. Chem.* **2014**, *57*, 5777–5791.

(23) Maiti, S.; Park, N.; Han, J. H.; Jeon, H. M.; Lee, J. H.; Bhuniya, S.; Kang, C.; Kim, J. S. *J. Am. Chem. Soc.* **2013**, *135*, 4567–4572.

(24) (a) Kim, T.; Jeon, H. M.; Le, H. T.; Kim, T. W.; Kang, C.; Kim, J. S. *Chem. Commun.* **2014**, *50*, 7690–7693. (b) Park, S.; Kim, E.; Kim, W. Y.; Kang, C.; Kim, J. S. *Chem. Commun.* **2015**, *51*, 9343–9345.

(25) Bhuniya, S.; Maiti, S.; Kim, E.-J.; Lee, H.; Sessler, J. L.; Hong, K. S.; Kim, J. S. *Angew. Chem., Int. Ed.* **2014**, *53*, 4469–4474.

(26) Wang, D.; Lippard, S. J. *Nat. Rev. Drug Discovery* **2005**, *4*, 307–320.

(27) Farrell, N. P. *Chem. Soc. Rev.* **2015**, *44*, 8773–8785.

(28) (a) Pathak, R. K.; Marrache, S.; Choi, J. H.; Berding, T. B.; Dhar, S. *Angew. Chem., Int. Ed.* **2014**, *53*, 1963–1967. (b) Pathak, R. K.; Dhar, S. *J. Am. Chem. Soc.* **2015**, *137*, 8324–8327.

(29) (a) Pizarro, A. M.; McQuitty, R. J.; Mackay, F. S.; Zhao, Y.; Woods, J. A.; Sadler, P. J. *ChemMedChem* **2014**, *9*, 1169–1175. (b) Butler, J. S.; Woods, J. A.; Farrer, N. J.; Newton, M. E.; Sadler, P. J. *J. Am. Chem. Soc.* **2012**, *134*, 16508–16511.

(30) Thiabaud, G.; Arambula, J. F.; Siddik, Z. H.; Sessler, J. L. *Chem. - Eur. J.* **2014**, *20*, 8942–8947.

(31) Presa, A.; Brissos, R. F.; Caballero, A. B.; Borilovic, I.; Korrodi-Gregório, L.; Pérez-Tomás, R.; Roubeau, O.; Gamez, P. *Angew. Chem., Int. Ed.* **2015**, *54*, 4561–4565.

(32) Naik, A.; Rubbiani, R.; Gasser, G.; Spingler, B. *Angew. Chem., Int. Ed.* **2014**, *53*, 6938–6941.

(33) (a) Mitra, K.; Basu, U.; Khan, I.; Maity, B.; Kondaiah, P.; Chakravarty, A. R. *Dalton Trans.* **2014**, *43*, 751–763. (b) Cummings, S. D. *Coord. Chem. Rev.* **2009**, *253*, 449–478. (c) Wang, W.; Yang, H.-B. *Chem. Commun.* **2014**, *50*, 5171–5186. (d) Chen, L.-J.; Zhang, J.; He, J.; Xu, X.-D.; Wu, N.-W.; Wang, D.-X.; Abliz, Z.; Yang, H.-B. *Organometallics* **2011**, *30*, 5590–5594.

(34) Mitra, K.; Patil, S.; Kondaiah, P.; Chakravarty, A. R. *Inorg. Chem.* **2015**, *54*, 253–264.

(35) Mitra, K.; Gautam, S.; Kondaiah, P.; Chakravarty, A. R. *Angew. Chem., Int. Ed.* **2015**, *54*, 13989–13993.

(36) (a) Sgambellone, M. A.; David, A.; Garner, R. N.; Dunbar, K. R.; Turro, C. *J. Am. Chem. Soc.* **2013**, *135*, 11274–11282. (b) Singh, T. N.; Turro, C. *Inorg. Chem.* **2004**, *43*, 7260–7262.

(37) Ow, F. P.; Djurovich, P. I.; Thompson, M. E.; Zink, J. I. *Inorg. Chem.* **2008**, *47*, 2389–2395.

(38) Shi, J.-F.; Wu, P.; Jiang, Z.-H.; Wei, X.-Y. *Eur. J. Med. Chem.* **2014**, *71*, 219–228.

(39) Cordero, F. M.; Bonanno, P.; Chioccioli, M.; Gratteri, P.; Robina, I.; Moreno Vargas, A. J.; Brandi, A. *Tetrahedron* **2011**, *67*, 9555–9564.

(40) Becke, A. D. *Phys. Rev. A: At., Mol., Opt. Phys.* **1988**, *38*, 3098–3100.

(41) Becke, A. D. *J. Chem. Phys.* **1993**, *98*, 5648–5652.

(42) Lee, C.; Yang, W.; Parr, R. G. *Phys. Rev. B: Condens. Matter Mater. Phys.* **1988**, *37*, 785–789.

DOI: 10.1021/acs.inorgchem.6b00680
Inorg. Chem. XXXX, XXX, XXX–XXX

(43) Frisch, M. J. et al. *Gaussian 09*, revision A.1; Gaussian, Inc.: Wallingford, CT, 2009 (see the Supporting Information for the full citation).
(44) Bernadou, J.; Pratviel, G.; Bennis, F.; Girardet, M.; Meunier, B. *Biochemistry* **1989**, *28*, 7268−7275.
(45) Hutchison, K.; Morris, J. C.; Nile, T. A.; Walsh, J. L.; Thompson, D. W.; Petersen, J. D.; Schoonover, J. R. *Inorg. Chem.* **1999**, *38*, 2516−2523.
(46) Higgins, S. L. H.; Brewer, K. J. *Angew. Chem., Int. Ed.* **2012**, *51*, 11420−11422.
(47) Siemeling, U.; Vor der Brüggen, J.-V.; Vorfeld, U.; Neumann, B.; Stammler, A.; Stammler, H.-G.; Brockhinke, A.; Plessow, R.; Zanello, P.; Laschi, F.; Fabrizi de Biani, F. F.; Fontani, M.; Steenken, S.; Stapper, M.; Gurzadyan, G. *Chem. - Eur. J.* **2003**, *9*, 2819−2833.
(48) Sathyaraj, G.; Kiruthika, M.; Weyhermüller, T.; Unni Nair, B. *Organometallics* **2012**, *31*, 6980−6987.
(49) Wu, K.-Q.; Guo, J.; Yan, J.-F.; Xie, L.-L.; Xu, F.-B.; Bai, S.; Nockemann, P.; Yuan, Y.-F. *Organometallics* **2011**, *30*, 3504−3511.
(50) Nakamoto, K. *Infrared and Raman Spectra of Inorganic and Coordination Compounds*, 3rd ed.; John Wiley & Sons: New York, 1978.
(51) Dong, T.-Y.; Shih, H.-W.; Chang, L.-S. *Langmuir* **2004**, *20*, 9340−9347.
(52) Yamaguchi, Y.; Kutal, C. *Macromolecules* **2000**, *33*, 1152−1156.
(53) Tan, Y. L. K.; Pigeon, P.; Hillard, E. A.; Top, S.; Plamont, M.-A.; Vessières, A.; McGlinchey, M. J.; Müller-Bunz, H.; Jaouen, G. *Dalton Trans.* **2009**, 10871−10881.
(54) Yamaguchi, Y.; Ding, W.; Sanderson, C. T.; Borden, M. L.; Morgan, M. J.; Kutal, C. *Coord. Chem. Rev.* **2007**, *251*, 515−524.
(55) (a) Mudasir; Yoshioka, N.; Inoue, H. *Transition Met. Chem.* **1999**, *24*, 210−217. (b) Hurvois, J. P.; Moinet, C. *J. Organomet. Chem.* **2005**, *690*, 1829−1839.
(56) Yamaguchi, Y.; Kutal, C. *Inorg. Chem.* **1999**, *38*, 4861−4867.
(57) Peña, L. A.; Seidl, A. J.; Cohen, L. R.; Hoggard, P. E. *Transition Met. Chem.* **2009**, *34*, 135−141.
(58) (a) Moon, S. J.; Kim, J. M.; Choi, J. Y.; Kim, S. K.; Lee, J. S.; Jang, H. G. *J. Inorg. Biochem.* **2005**, *99*, 994−1000. (b) Peyratout, C. S.; Aldridge, T. K.; Crites, D. K.; McMillin, D. R. *Inorg. Chem.* **1995**, *34*, 4484−4489.
(59) Burrows, C. J.; Muller, J. G. *Chem. Rev.* **1998**, *98*, 1109−1152. Szacilowski, K.; Macyk, W.; Drzewiecka-Matuszek, A.; Brindell, M.; Stochel, G. *Chem. Rev.* **2005**, *105*, 2647−2694.
(60) Balaji, B.; Balakrishnan, B.; Perumalla, S.; Karande, A. A.; Chakravarty, A. R. *Eur. J. Med. Chem.* **2015**, *92*, 332−341.
(61) Gandioso, A.; Shaili, E.; Massaguer, A.; Artigas, G.; González-Cantó, A.; Woods, J. A.; Sadler, P. J.; Marchán, V. *Chem. Commun.* **2015**, *51*, 9169−9172.
(62) Sun, R. W.-Y.; Ma, D.-L.; Wong, E. L.-M.; Che, C.-M. *Dalton Trans.* **2007**, 4884−4892.
(63) Trajkovski, M.; Morel, E.; Hamon, F.; Bombard, S.; Teulade-Fichou, M.-P.; Plavec, J. *Chem. - Eur. J.* **2015**, *21*, 7798−7807.
(64) Ma, D.-L.; Shum, T. Y.-T.; Zhang, F.; Che, C.-M.; Yang, M. *Chem. Commun.* **2005**, 4675−4677.
(65) Harper, B. W. J.; Aldrich-Wright, J. R. *Dalton Trans.* **2015**, *44*, 87−96.

DOI: 10.1021/acs.inorgchem.6b00680
Inorg. Chem. XXXX, XXX, XXX−XXX